Center for Advanced Materials

CAM

Presented at the International Cryogenic Materials '89 Conference, Los Angeles, CA, July 24–28, 1989, and to be published in the Proceedings

The Effects of Temperature on Fatigue Crack Propagation in 310 Austenitic Stainless Steel

Z. Mei, J.W. Chan, and J.W. Morris, Jr.

July 1989

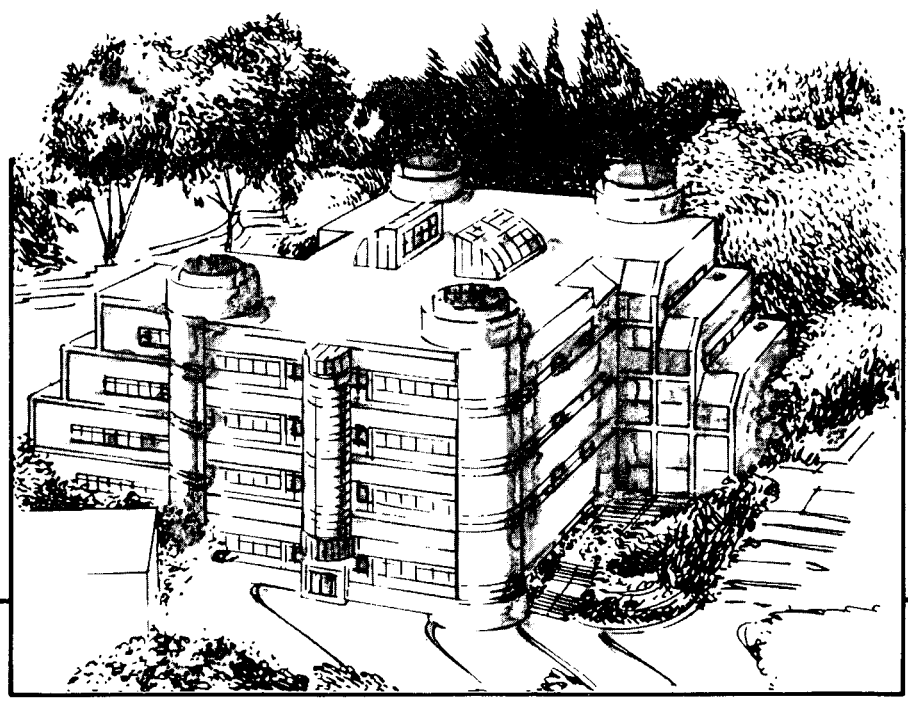

Materials and Chemical Sciences Division

Lawrence Berkeley Laboratory • University of California

ONE CYCLOTRON ROAD, BERKELEY, CA 94720 • (415) 486-4755

Prepared for the U.S. Department of Energy under Contract DE-AC03-76SF00098

DISCLAIMER

LBL 27375

The Effects of Temperature on Fatigue Crack Propagation in 310 Austenitic Stainless Steel

Z. Mei, J. W. Chan, and J. W. Morris, Jr.

Center for Advanced Materials
Materials and Chemical Sciences Division
Lawrence Berkeley Laboratory
University of California

and

Department of Materials Science and Mineral Engineering
University of California at Berkeley
Berkeley, California 94720

July 1989

This work was supported by the Director, Office of Energy Research, Office of Fusion Energy, Development and Technology Division of the U.S. Department of Energy, under Contract No. DE-AC03-76SF00098.

The Effects of Temperature on Fatigue CrackPropagation in 310 Austenitic Stainless Steel

Z. Mei, J. W. Chan, and J. W. Morris, Jr.

Center for Advanced Materials, Lawrence Berkeley Laboratory and
Department of Materials Science and Mineral Engineering,
University of California at Berkeley

The fatigue crack propagation rate of 310 austenitic stainless steel was measured at 298 K, 77 K, and 4 K. As temperature decreased the fatigue crack growth rate decreased while the threshold stress intensity increased. At all three temperatures the fatigue crack propagated in a quasi-cleavage mode along a zigzag path. The propagating crack branched to an extent that increased as the temperature decreased. Since no martensite was detected on the crack surfaces and the crack surfaces were smoother at lower temperatures, neither transformation toughening nor roughness-induced crack closure can account for the temperature dependance of the crack growth rate. Various factors that might contribute to the temperature dependence are discussed.

INTRODUCTION

The structural materials used in a superconducting magnet in a fusion reactor must sustain high cyclic stresses at cryogenic temperatures.[1] The design of such structures requires an understanding of fatigue crack propagation behavior at cryogenic temperatures. Austenitic stainless steels are often the structural materials of choice. In previous work [14,15] we have studied fatigue crack growth in metastable austenitic steels. The present work addresses fatigue crack growth in a stable austenitic stainless steel, alloy 310, at temperatures between 4 and 298 K, to examine the behavior of austenitic material in the absence of a phase transformation.

Fatigue crack propagation in the threshold region at low temperatures has been studied for several alloys[2-16], including Al alloys, Cu alloys, austenitic stainless steels, mild steels, high strength low alloy steel, JBK-75 stainless steel, and inconel 706. It was found that the threshold cyclic stress intensity increases and the near-threshold crack growth rate decreases as the temperature decreases from 298 K to 4 K. This behavior has been attributed to surface-roughness-induced crack closure[10], transformation toughening[14,15], and thermally activated dislocation movement.[11]

In contrast to the trend found in the threshold region, the crack growth rate in the Paris-law region may either increase or decrease with the temperature. The relevant data was recently reviewed by Tobler and Cheng[17], who summarize results for more than 200

material and temperature combinations, including ferritic nickel steels, austenitic stainless steels, Ni-base superalloys, Ti-base alloys, and Al-base alloys. For most alloys the slope of the logarithmic fatigue crack growth rate, that is, the parameter (n) in the Paris Law: $da/dN = A\ (\Delta K)^n$, increases as the temperature decreases. The value of (n) for most metals at 298 K is in the range 2 - 4, and may increase to 5 - 8 at cryogenic temperature. The increase in (n) reflects the fact that materials become more brittle as the temperature decreases; for example, the value of (n) is more than 100 for ceramics.[18] The conventional AISI 300 series austenitic stainless steels were not found to exhibit an increase in (n) with decreasing temperatures.[19]

EXPERIMENTAL PROCEDURE

The chemical composition of the commercial grade AISI 310 stainless steel used in this study was, in weight percent, 24.73Cr-19.23Ni-1.73Mn-0.51Si-0.26Mo-0.16Cu-0.15Co-0.066N-0.021C-0.023P-0.008S. The steel was annealed at 1050 C for 1 hour and then quenched in water. The grain size was ≈100 mm (Fig. 2).

The fatigue crack growth rate was determined for a 12.7 mm thick compact tension specimen. The specimens were tested under load control in a hydraulic testing machine, using a sine-wave load form and frequencies of 10 - 20 Hz. The crack length was monitored continuously using the direct current electrical potential method.[20] The relation between a/W (crack length / specimen width) and V/V_0 (voltage at a / voltage at a_0, initial crack length) was determined at both 298 K and 77 K. The relations at both temperatures are almost the same, as expected. While the complete calibration curve was not measured at 4 K, a comparison of the final crack length and the length as determined from the 77 K calibration curve shows good agreement (<5%). The cyclic stress intensity factor was calculated from the crack length and cyclic load as suggested in the ASTM standard .[21] The near-threshold region of the fatigue crack propagation curve was measured under decreasing cyclic load, ΔP, using a step-wise decrement in ΔP of less than 7% per step. At each load level the crack was allowed to propagate a distance at least 3 times the computed maximum plastic zone size formed at the previous ΔP level. After establishing the threshold, ΔP was increased step-wise and da/dN values were recorded until the specimen sustained general yield. The tests at 77 K and 4 K were done by immersing the samples in liquid nitrogen and liquid helium. The extent of crack closure during fatigue crack growth was monitored continuously using the back-face strain gauge technique.[22]

The fatigue crack profiles were observed by optical microscopy. The sample was sectioned perpendicular to the crack plane at center thickness, mechanically polished, and chemically etched (15 ml HNO_3 - 45 ml HCl - 20 ml CH_2OH). The fatigue fracture surfaces were studied by scanning electron microscopy (SEM) to determine fracture mode, by X-ray diffractometry to check for evidence of phase transformation, and by surface profilometry to characterize surface roughness.

RESULTS

Fig. 1 includes measured fatigue crack growth curves for 310 austenitic stainless steel at room temperature (RT), liquid nitrogen temperature (LNT), and liquid helium temperature (LHT). The parameters n and A in the Paris Law formula ($da/dN = A\,\Delta K^n$) are: at RT, n = 3.79, A = 1.50 x 10^{-9} mm/cycle; at LNT, n = 3.67, A = 8.45 x 10^{-10} mm/cycle; at LHT, n = 4.51, A = 7.97 x 10^{-12} mm/cycle. There is a real, but small increase in (n) at LHT compared with the (n) values at LNT and RT. The threshold cyclic stress intensity was 3.5 MPa-$m^{1/2}$ at RT and 4.8 MPa-$m^{1/2}$ at LNT.

The results differ somewhat from those reported by Tobler et al. [23] for the same material. They found essentially equal crack growth rates, da/dN, at LNT and LHT which were about one-half those measured at RT for the same ΔK. Moreover, their crack growth rates were uniformly lower than those measured here; if their RT data were plotted in Fig. 1, it would appear just on the right side of our 310 LHT data line. However, their data include only a small section (between 3 x 10^{-6} to 2 x 10^{-4} mm/cycle) of the whole fatigue propagation curve. It may also be relevant that their fatigue specimen thickness was between 25.4 mm and 50.8 mm (1 in - 2 in) while ours was 12.7 mm (0.5 in). In earlier work, we did observe a specimen thickness effect on the fatigue crack propagation in 304L austenitic stainless steel; however the magnitude of this effect seems too small to explain the large difference between their data and the current data.

The fatigue curves of 304L austenitic stainless steel at RT and LNT[14], are also plotted in Fig. 1. For this alloy, the increase in the threshold stress intensity range and the reduction in the crack growth rate with decreasing temperature is a result of the deformation-induced martensitic transformation that occurs at LNT in addition to inherent temperature effects. Alloy 310 remains austenitic when tested at RT, LNT, and LHT, yet also shows an increase in the threshold stress intensity range and a reduction in the crack growth rate with decreasing temperature.

Optical microscopy revealed that fatigue cracks propagate in 310 stainless steel in a zigzag path. The cracks are kinked and branch at all temperatures. Crack branching is most prominent at LHT as shown in Fig. 2. The direction of crack propagation almost invariably changes at grain boundaries, and may also change within a single grain to produce a sawtooth pattern. The crack path appears to be a consequence of two competing tendencies: preferential crack growth along particular crystallographic planes, and maximal driving force for crack propagation perpendicular to the axis of loading. The result is a zigzag path. Kinks and branches reduce the crack growth rate for two reasons: the crack passes through a longer distance along a zigzag path than along a straight path, and the effective stress intensity factor is smaller if the crack deviates from the plane normal to the external load.[23]

Fig. 3(a)-(d) are scanning electron micrographs of the fatigue fracture surfaces. The crack propagation directions are marked by arrows. For the specimen tested at RT, fatigue striations are easily seen when ΔK is larger than $\approx$ 32 MPa-$m^{1/2}$. The striation spacing is close to the crack extension per cycle. It is interesting that the striations have

different orientations in different grains, for example grain A and B in Fig. 3(a). Fatigue striations were not seen in the specimens tested at LNT and LHT. When ΔK is smaller than ≈ 32 MPa-$m^{1/2}$, the fracture surface at RT resembles that at LNT and LHT. At all three temperatures, the cracks propagate in a quasi-cleavage mode. As shown in Fig. 3(b) and 3(c) the flow of the river pattern is in the direction of crack propagation, and the pattern changes across grain boundaries. These features are characteristic of the cleavage fracture mode.[24] Note that the crack profile, Fig. 2, also shows that the crack changes its propagation direction across grain boundaries .

No crack closure was detected during the fatigue tests at RT and LNT by the back-face strain gauge technique, although the measurement of surface roughness and observation of crack profile led us to believe that crack closure should occur. An experimental error with the back-face strain gauge prevented the study of closure at LHT.

To clarify the influence of surface roughness on fatigue crack propagation the fracture surfaces of the fatigue specimens were characterized by profilometry. Fig. 4 shows two line scans for each of three specimens tested at RT, LNT, and LHT. The profilometer scanning direction was along the fatigue crack propagation direction. The roughness of the surfaces was quantified by the parameter R defined as

$$R = \frac{\int_0^L |y(x) - \bar{y}|\,dx}{L} \qquad (1)$$

where y (x) is the surface line-scanning data denoting the surface height y as function of horizontal position x, $\bar{y}$ is the average surface height, L is the line-scanning distance. The results document the decrease in roughness as the temperature decreases. The roughness of the fatigue fracture surface should depend on the grain size, fracture mode, and the amount of plastic deformation during fracture. Observations of the fracture surface (Fig. 3) and the crack profile (Fig. 2) indicate that at all three temperatures (RT, LNT, and LHT) the fatigue crack extends in a quasi-cleavage mode. The roughness of the fatigue fracture surface is then decided by the plasticity. The larger the plastic zone size (as the temperature increases), the rougher the fracture surface becomes.

The results of X-ray diffraction measurements of the fatigue fracture surfaces confirm our expectation that 310 austenitic stainless steel is stable with respect to deformation-induced martensite at cryogenic temperatures. Fig. 5(a) shows the diffraction data for the LHT fatigue specimen. No martensite peaks appear. But the X-ray diffraction data is of interest in another respect. Comparing the spectrum of the fatigue fracture surface (Fig. 5(a)) with that of the surface 3 mm below the fatigue fracture surface (Fig. 5(b)), we see an increase in intensity of the 002 peak. This same phenomenon was observed on the LNT and RT fatigue specimens, and may indicate the development of a preferential texture as a result of the plastic deformation near the crack tip. While it is well known that a preferential texture develops during monotonic straining, the development of texture during cyclic plastic strain has not been studied. Another possibility is that the

crack propagates preferentially along 002 crystallographic planes to create a fracture surface that exposes many 002 planes. These two possible explanations are currently under further investigation.

DISCUSSION

The fatigue crack propagation rate of 310 austenitic stainless steel decreases and threshold cyclic stress intensity increases as the temperature decreases from RT to LHT. Two mechanisms have been proposed to explain this effect. The first is crack closure, which, as discussed above, is not observed to a significant degree in the present experiments. A second possible explanation for the temperature dependance relates it to the thermal activation of the dislocation motion that drives plastic crack extension. Models of fatigue crack propagation through the dynamic motion of dislocations have been proposed by Yokobori et al.[25] and by Gerberich et al.[26] and successfully explain some experimental data.[11,27] In these models the dislocation movement is related to the crack extension. Since the dislocation movement is a thermally activated process, the crack propagation is also thermally activated with the same activation energy. If these models apply a plot of ln(da/dN) vs. 1/T should be a straight line with a slop equal to the activation energy, Q, for thermally activated dislocation motion. As shown in Fig. 6, however, the data are not linear on a plot of this type. The nonlinear relation between ln(da/dN) and 1/T suggests that the rate of fatigue crack propagation is not limited by thermally activated dislocation motion.

The data obtained here makes it appear that the fatigue crack growth behavior of alloy 310 is limited by the metallurgy of the alloy, and closely associated with the fracture mode. As temperature decreases crack propagation is increasingly anisotropic. The fracture surfaces are made up of relatively flat facets on well-defined crystallographic planes. The deviation of the preferred plane from the plane of maximum tension and the increasing degree of branching at low temperature reduce the driving force for crack propagation, raising the threshold value and decreasing the crack growth rate.

While anisotropy in the crack growth is the most evident feature that affects the fatigue behavior of alloy 310, it should be kept in mind that its behavior is not anomalous. The threshold value of the cyclic stress intensity increases as the temperature drops in almost all alloys.[2-16] The increase in the exponent (n) is also a common observation.[17] These observations suggest that there are common underlying factors governing the threshold and crack growth exponent that remain to be understood.

ACKNOWLEGEMENT

The authors are grateful to S. Shaffer, D. Tribula, S. Takaki, and J. Schmitt for assistance in the experiments and helpful discussions. This work was supported by the Director, Office of Energy Research, Office of Fusion Energy, Development and Technology Division of the U.S. Department of Energy, under Contract No. DE-AC03-76SF00098.

REFERENCES

1. L. Summers, Lawrence Livermore National Laboratory, private communication, 1989.

2. P. K. Liaw and W. A. Logsdon, Acta Metall., 36:1731 (1988).

3. J. Mckittrick, P. K. Liaw, S. I. Kwun, and M. E. Fine, Metall. Tran. A, 12:1535 (1981).

4. P. K. Liaw, W. A. Logsdon, and M. H. Attaar, "Fatigue at Low Temperatures", ASTM STP 857, R. I. Stephens, ed., ASTM, Philadelphia, (1985), p. 173.

5. P. K. Liaw and W. A. Logsdon, Engineering Fracture Mechanics, 22:585 (1985).

6. E. Tschegg and S. Stanzl, Acta Metall., 29:33 (1981).

7. J. P. Lucas and W. W. Gerberich, Materials Science and Engineering, 51:203 (1981).

8. K. A. Esaklul, W. K. Yu, and W. W. Gerberich, "Fatigue at Low Temperatures", ASTM STP 857, R. I. Stephens, ed., ASTM, Philadelphia, (1985), p. 63.

9. V. K. Jata, W. W. Gerberich, and C. J. Beevers, "Fatigue at Low Temperatures", ASTM STP 857, R. I. Stephens, ed., ASTM, Philadelphia, (1985), p. 102.

10. W. W. Gerberich, W. Yu, and K. Esaklul, Metall. Tran. A, 15:875 (1984).

11. W. Yu, K. Esaklul, and W. W. Gerberich, Metall. Tran. A, 15:889 (1984).

12. R. L. Tobler and Y. W. Cheng, Int. J. Fatigue, 7:191 (1985).

13. R. L. Tobler, Adv. Cryog. Eng., 32:321 (1986).

14. Z. Mei, G. M. Chang, and J. W. Morris, Jr., "Cryogenic Materials '88", R. P. Reed, Z. S. Xing, and E. W. Collings, eds., ICMC, Boulder, Colorado (1988), Vol. 2, p. 491.

15. Z. Mei and J. W. Morris, Jr., to be published in Metall. Trans. A.

16. J. Glazer, S. L. Verzasconi, E. N. C. Dalder, W. Yu, R. A. Emigh, R. O. Ritchie, and J. W. Morris, Jr., Adv. Cryog. Eng., 32:397 (1986).

17. R. Tobler and Y. Cheng, "Fatigue at Low Temperatures", ASTM STP 857, R. I. Stephens, ed., ASTM, Philadelphia, (1985), p. 5.

18. R. H. Dauskardt, D. B. Marshall, and R. O. Ritchie, to be published in J. Am. Ceram. Soc..

19. Y. Cheng and R. Tobler, Proceedings of ICF International Symposium on Fracture Mechanics, D. Tan and D. Chen , eds., Science Press, Beijing, China (1983), 635.

20. "Metals Handbook", 9th edition, ASTM, Philadelphia, PA (1983), Vol. 8, p. 386.

21. "Annual Book of ASTM Standards", E 647-83, ASTM, Philadephia, PA (1983), p.739.

22. R. O. Ritchie and W. Yu, "Small Fatigue Cracks", R. O. Ritchie and J. Lankford, eds., TMS-AIME, Warrendale, PA (1986), p. 167.

23. R. L. Tobler, R. P. Mikesell, R. L. Durcholz, and R. P. Reed, "Semi-Annual Report", NBS (October,1974).

23. S. Suresh, Metall. Trans. A, 14:2375 (1983).

24. R. W. Hertzberg, "Deformation and Fracture Mechanics of Engineering Materials", second edition, John Wiley & Sons, Inc. (1983), p. 255.

25. T. Yokobori, S. Konosu, and A. T. Yokobori, Jr., "Proceedings, International Conference of Fracture, Vol. 1, Pergamon Press, New York (1978), p.665.

26. W. W. Gerberich and K. A. Peterson, "Micro and Macro Mechanics of Crack Growth", K. Sadananda, B. B. Rath, and D. J. Michel, eds., TMS-AIME, Warrendale, PA (1982), p. 1.

27. T. Yokobori, I. Maekawa, Y. Tanabe, Z. Jin, and S. I. Nishida, "Fatigue at Low Temperatures", ASTM STP 857, R. I. Stephens, ed., ASTM, Philadelphia, (1985), p. 121.

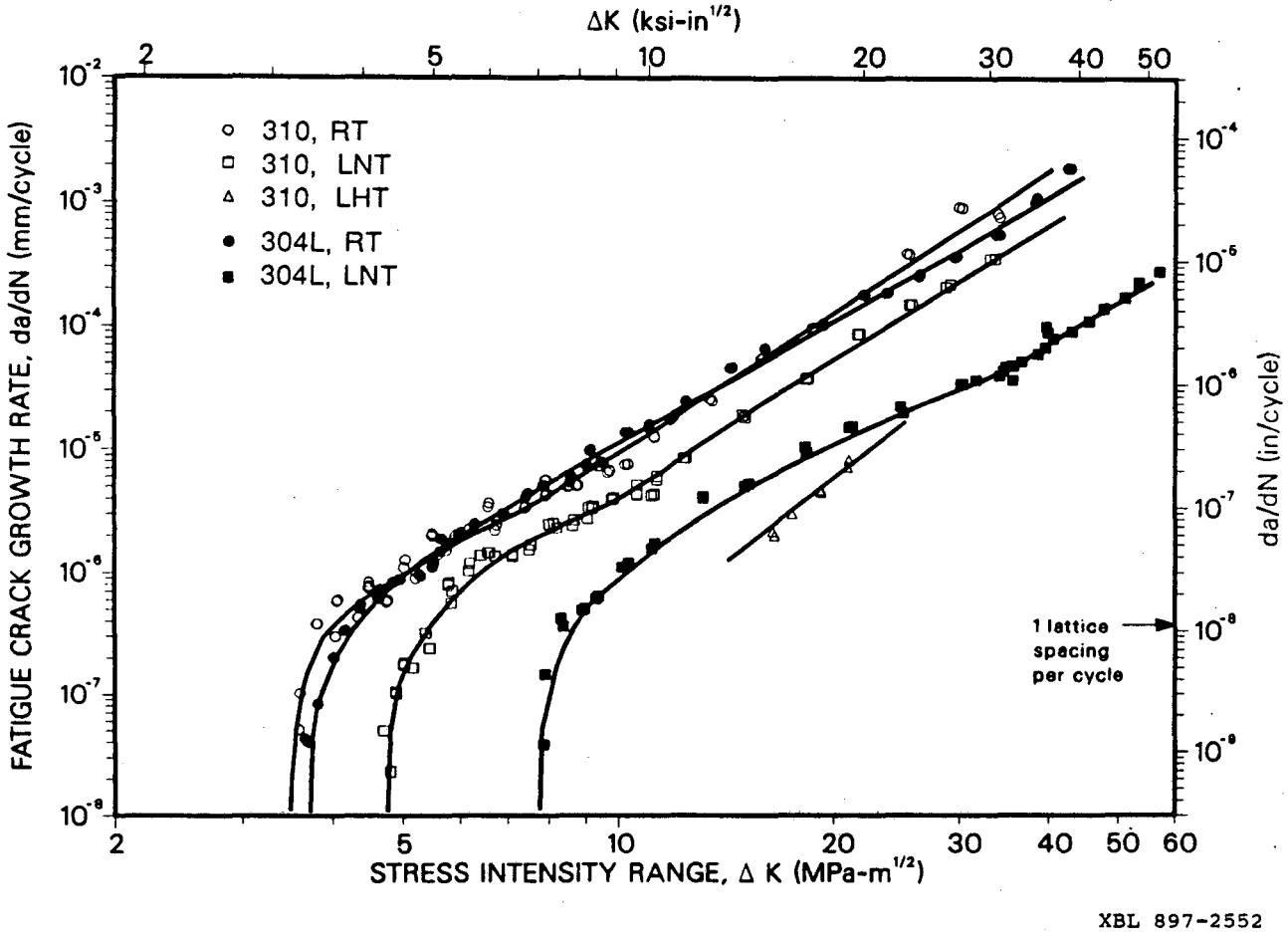

Fig. 1: Fatigue crack propagation curves of 310 and 304L austenitic stainless steels at room temperature (RT), liquid nitrogen temperature (LNT), and liquid helium temperature (LHT).

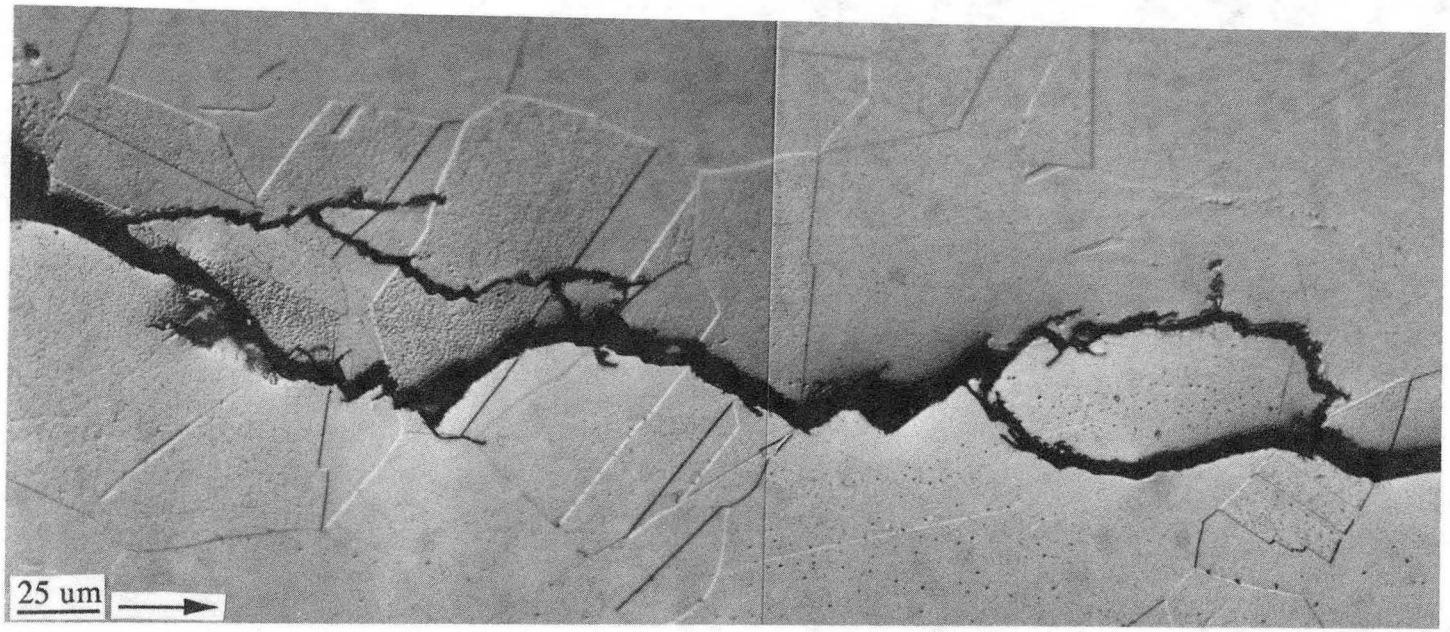

Fig. 2: Optical micrograph of the fatigue crack profile of the specimen tested at liquid helium temperature.

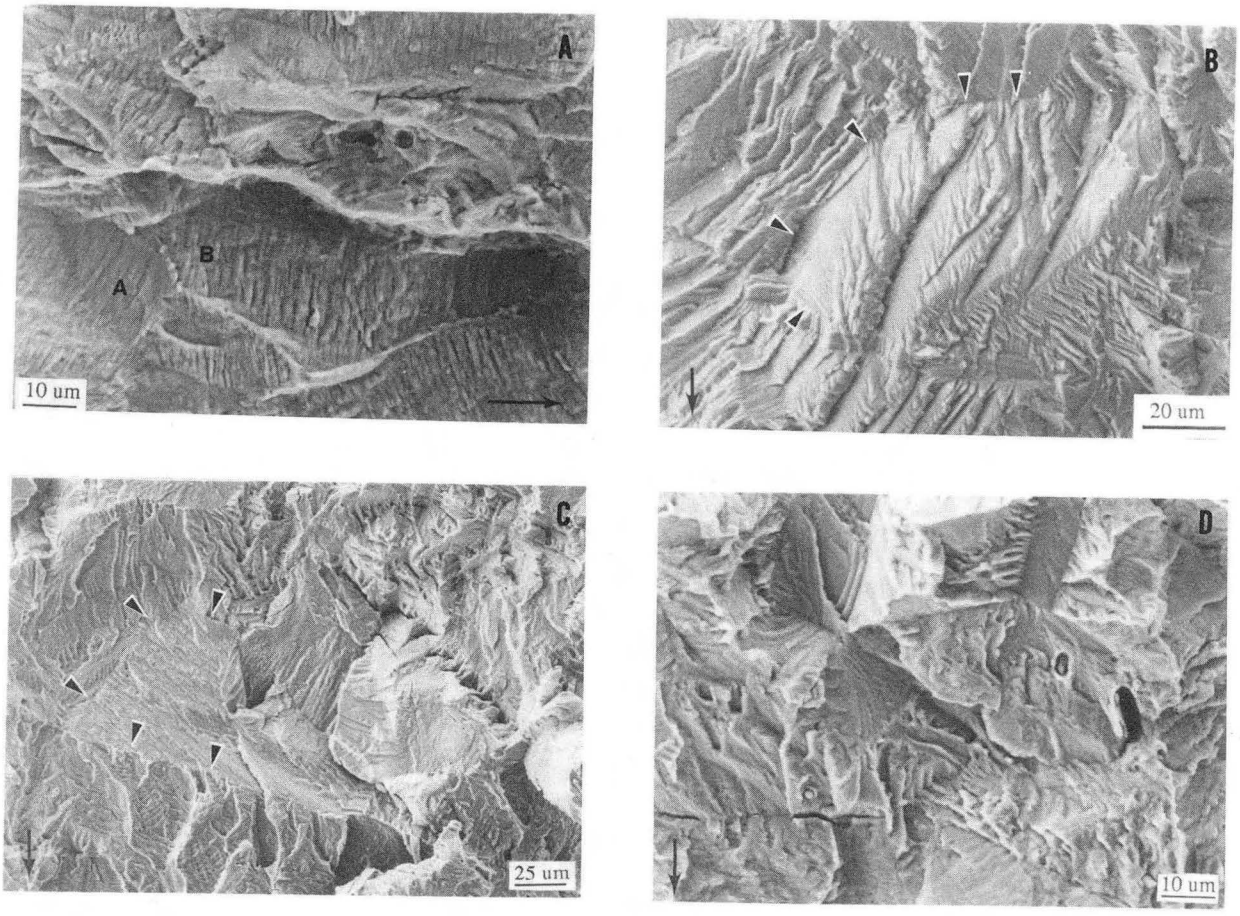

Fig. 3: Scanning electron micrographs of the fatigue fracture surfaces of the specimens under the conditions of (a) room temperature, $\Delta K \approx 32$ MPa-$m^{1/2}$, $da/dN \approx 1$ μm/cycle; (b) liquid nitrogen temperature, $\Delta K \approx 10.5$ MPa-$m^{1/2}$, $da/dN \approx 1.1 \times 10^{-2}$ μm/cycle; (c) liquid helium temperature, $\Delta K \approx 20$ MPa-$m^{1/2}$, $da/dN \approx 7 \times 10^{-3}$ μm/cycle; (d) liquid helium temperature, $\Delta K \approx 20$ MPa-$m^{1/2}$, $da/dN \approx 7 \times 10^{-3}$ μm/cycle.

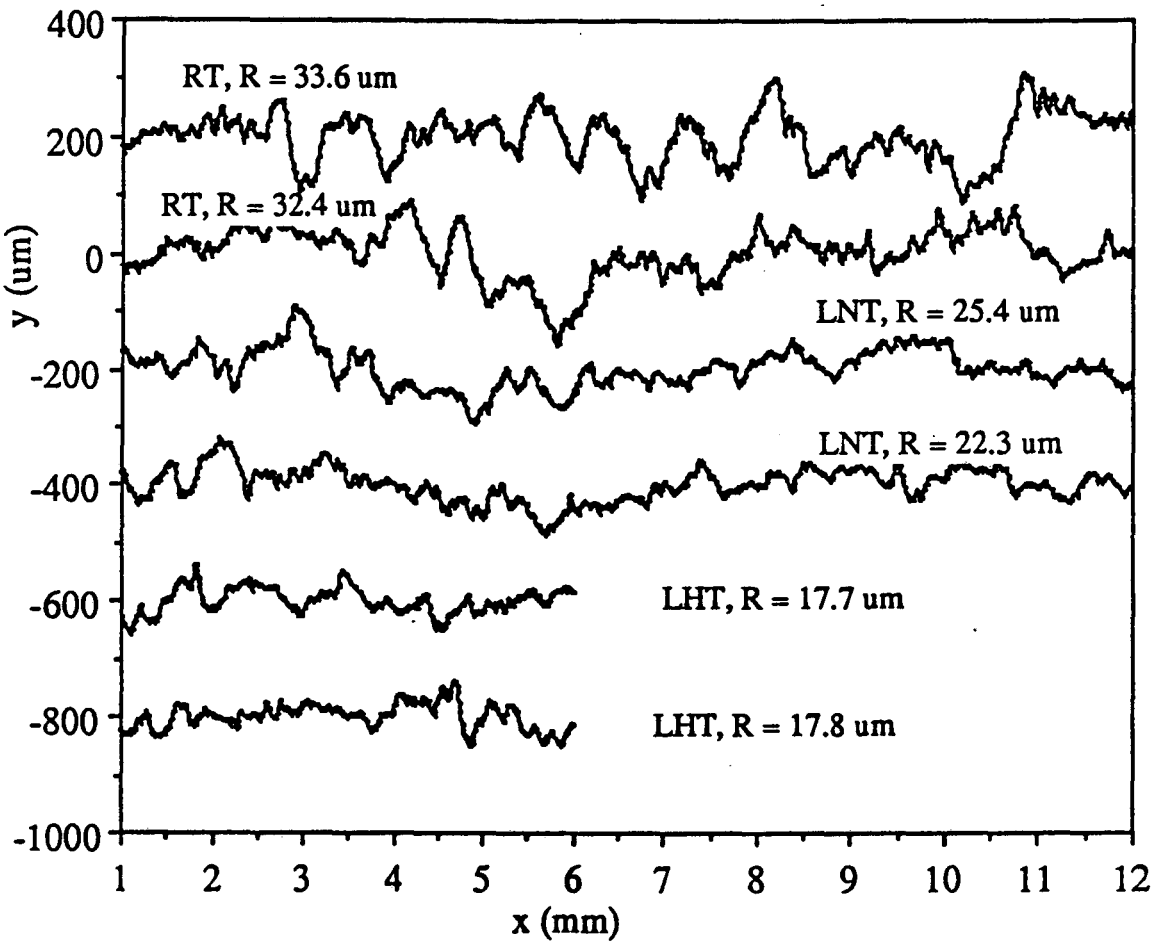

Fig. 4: Profilometer line scannings of the fatigue fracture surfaces of the specimens that were fatigue tested at room temperature (RT), liquid nitrogen temperature (LNT), and liquid helium temperature (LHT). Cracks propagated from right to left, the roughness parameter R is defined in the text.

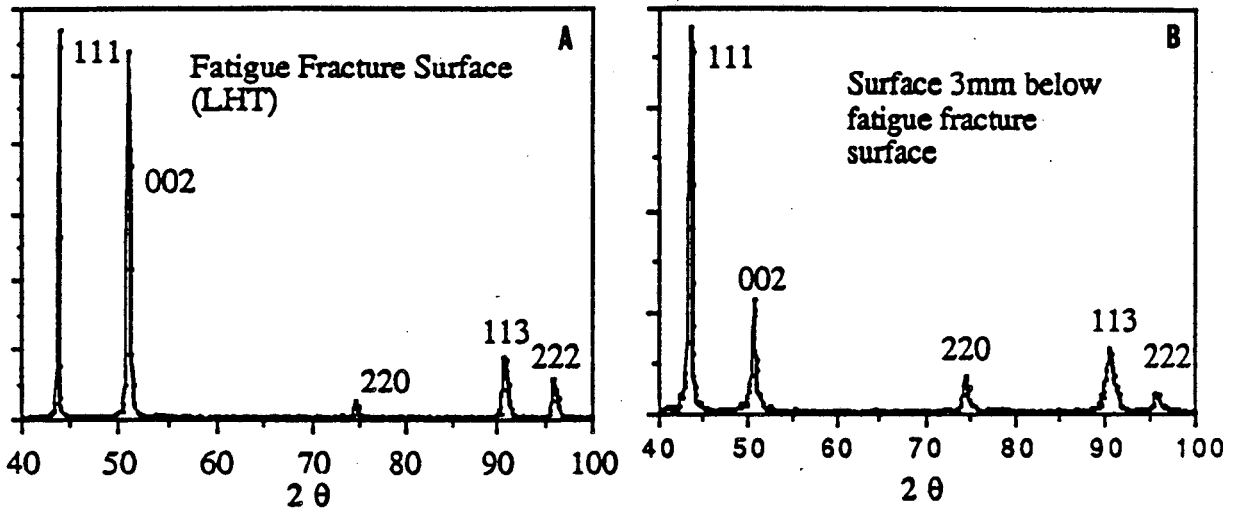

Fig. 5: X-ray diffraction data of (a) fracture surface of the fatigue specimen tested at liquid helium temperature (LHT) and (b) the surface 3mm below the frature surface.

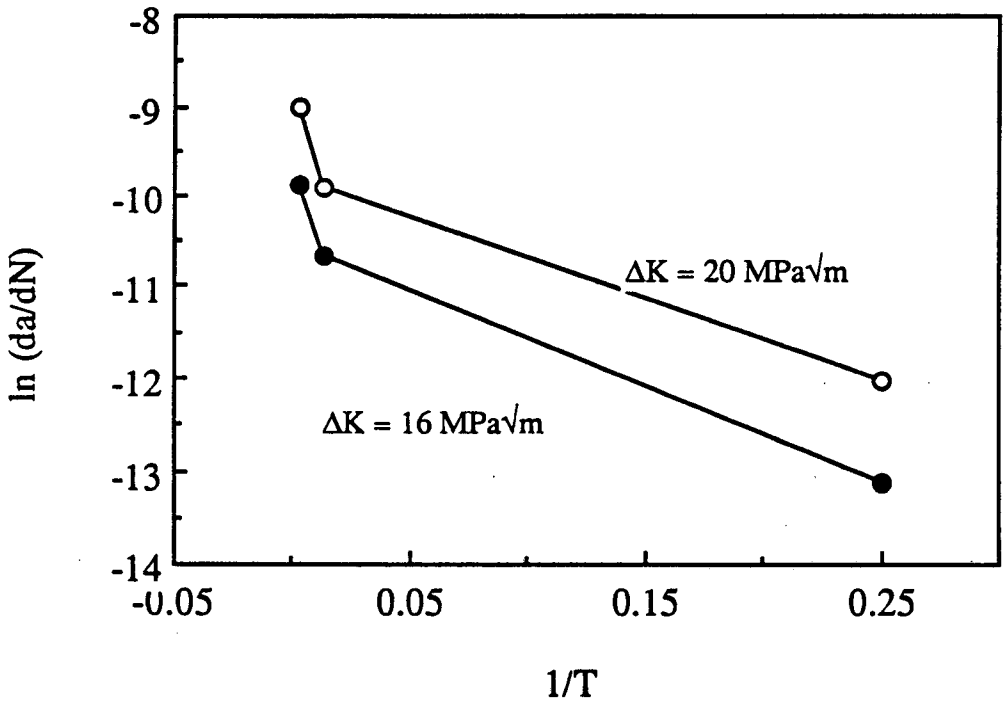

Fig. 6: Two plots of ln(da/dN) vs. 1/T at ΔK = 20 and 16 MPa-$m^{1/2}$.

LAWRENCE BERKELEY LABORATORY
CENTER FOR ADVANCED MATERIALS
1 CYCLOTRON ROAD
BERKELEY, CALIFORNIA 94720